IN SITU POTENTIOMETRIC, RESISTANCE, AND DILATOMETRIC MEASUREMENTS OF PALLADIUM ELECTRODES DURING REPEATED ELECTROCHEMICAL HYDROGEN ABSORPTION

NUCLEAR REACTIONS IN SOLIDS

KEYWORDS: *electrolytic hydrogen absorption, resistance measurement, dilatometry, void, Pd, phase transformation*

HIROO NUMATA* and IZUMI OHNO *Tokyo Institute of Technology*
Faculty of Engineering, 2-12-1, O-okayama, Meguro, Tokyo 152-8552, Japan

Received June 22, 1999
Accepted for Publication October 31, 1999

The physicochemical properties of the Pd-H system were studied by in situ potentiometric, resistance, and dilatometric measurements in each of three applied pulse modes, A, B, and C, and repeated H absorption and desorption. Potential, resistance ratio, and an increase in dilation ($\Delta l/l_0$) were measured simultaneously after H equilibrium was attained with the Pd electrode. During continuous absorption, structural phase transition ($\alpha \rightarrow \beta$) and void formation occurred, and the values of the H/Pd ratio in the limiting α phase, in the $\alpha + \beta$ phase coexistence, and in the transition and the β + voids coexistence regions are consistent with those obtained from the Pd-H isotherm at 40°C. Hydrogen absorption caused the dilation, from whose slope the molar volume was obtained as 0.64 (α phase) and 0.40 ($\alpha + \beta$ phase) cm^3/mol. The resistance increased in proportion to the H/Pd ratio and was kept constant at 1.7 to 1.8 over R_{tr}.

For the first absorption through the β phase ($>\beta_{min}$), the electrode potential shifted with an increase in dilation, which suggests nonequilibrium PdH_{2-x} precipitation followed by conversion to the β phase and void formation. Although there was a remarkable lack of any dependence on the number of repetitions of the values of the limiting resistance and potential corresponding to the $\alpha + \beta$ and β + void coexistence, the onset of the β phase, β_{min}, increased as the number of repetitions increased. The volumetric ratio for an increase in the H/Pd ratio corresponds to the absorption in high-density defect areas surrounding voids. During repeated absorption and desorption in the C applied pulse mode, the apparent molar volumes of the $\alpha + \beta$ phase coexistence show that absorption proceeds inhomogenously, in contrast to the first absorption in the A applied pulse mode.

I. INTRODUCTION

Since Fleischmann and Pons[1] and Jones et al.[2] reported the possibility of nuclear fusion during electrolytic loading of deuterium in Pd at ambient temperatures, much work[3–6] on reproducing nuclear fusion in condensed matter has been carried out. Fleischmann and Pons and Jones et al. suggested that the nuclear fusion reaction is caused by the absorption of deuterium in a Pd electrode. One of the reasons for this phenomenon might be a nuclear fusion reaction brought about by the dissolution of deuterium within a solid by means of high pressure. However in an equilibrium state, the pressure is no greater than ten or several tens of atmospheres, which is not sufficient for this case. In a nonequilibrium state, e.g., crack formation might provide an explanation. Takagi et al.[7] observed burstlike neutron emissions during long-term electrolysis on Pd (21-mm diameter, 32 mm long) in 0.1 *M* LiOD at current densities of 0.04 to 0.10 A/cm^2. Microscopic observation[8] of postelectrolysis Pd showed that long-term electrolysis for 8 months did not result in any cracking but caused many straight and cross slip bands, surface voids, and two long faults. The electrode microstructure after deuterium absorption showed that two large columnar crystals had grown along the longitudinal axis, one of which had a peculiar morphology: voids

*E-mail: numata@mtl.titech.ac.jp

arranged in a straight line. Besides these morphological findings, the electrode gradually expanded diametrally, resulting in 7.8 to 8.3% dilation during loading.

We have attempted to elucidate the elemental steps of electrochemical H absorption, i.e., infusion, diffusion, subsequent phase changes, lattice expansion, related resistance increase, etc., under well-defined electrolysis conditions. The entropy and enthalpy change of solution and the molar volume of H obtained by the electrochemical measurement are consistent with those of gas equilibrium experiments.[9,10] As the H/Pd ratio increases, the structural phase change ($\alpha \rightarrow \beta$) occurs, obeying the thermodynamic phase rule. The characteristic values of the phase change [α_{max}, β_{min}, $pH_2^{eq}(\alpha + \beta)$] are consistent with those of the Pd-H isotherm at 40°C, where α_{max} and β_{min} are the limits of the α phase and that of the $\alpha + \beta$ coexistence, and $pH_2^{eq}(\alpha + \beta)$ is the equivalent H pressure of the $\alpha + \beta$ coexistence. Prolonged discharge of deuterium on a Pd electrode has been shown to produce heavily worked features[8] that are different from those obtained in a single absorption run. Such microscopic morphology resembling a heavily worked specimen is attributed to the irreversible phase changes ($\alpha \rightarrow \beta$ and $\beta \rightarrow \alpha$) or to inhomogeneous plastic deformation during the H absorption and desorption runs. Since repeated H absorption followed by desorption might result in an accumulation of the mechanical stress generating miscellaneous structural defects, in situ measurements of the electrode potential, dilation, and resistance under well-controlled H absorption are of interest to evaluate the influence of absorption/desorption repetitions on the solid-state properties of Pd.

In this study, the electrochemical behavior, the dilation, and the resistance of the Pd electrode have been measured in situ using a computer-controlled potentiostat connected to the measurement devices. These measurements were made with respect to the microstructural changes induced by H ingress in the Pd electrode.

II. EXPERIMENT

The absorption and desorption of H in the Pd electrode (0.8- and 2-mm diameters, 50-mm length, 99.95% purity) were performed by applying galvanostatic cathodic and anodic pulsed currents at low current densities, $<2 \times 10^{-3}$ A/cm^2. As-received Pd rods were annealed at 800°C for 3 h under a flow of He. After heat treatment, the surface of the rods was polished with emery paper up to 1000 count and stored in a desiccator. Before being used, annealed samples were maintained in vacuo at 300°C overnight to eliminate the influence of residual H on the measurements. The mass was measured with a chemical balance, and the number of atoms of the electrode metal was obtained. Gold wire ~1 cm long was spot welded to one side of the electrode, and a lead was taken out with an enameled Cu wire. The welded parts were covered with silicone rubber filler.

The electrolyte was composed of glycerine and phosphoric acid (2:1 in volume ratio). Kirchheim[11] reported that out-diffusion of H during electrolysis is very slow when a solution with high viscosity is used, and the H, once dissolved within metal, is unlikely to leak out. The electrolyte was settled in an electrolytic cell with a sintered glass bubbler, through which dry N was bubbled for several hours for deoxygenation. A N atmosphere was maintained by pouring dry N over the upper side of the solution during measurements. The temperature was kept constant at 40 ± 0.5°C using an isothermal bath.

The electrolytic cell was a modified three-electrode cell, as shown in Fig. 1. A luggin capillary located at the electrode surface was used to measure the electrode potentials against a saturated calomel electrode (SCE). The counter electrode was made of a platinized plate (35 × 15 mm). A set of potential, dilation, and resistance measurements were made on the Pd electrode after the establishment of H equilibrium with Pd. The measurement system consisted of a computer-controlled potentiostat, milliohm meter, and dilatometer; placement of the measurement equipment is shown in Fig. 2.

To obtain each data point, the following procedure was undertaken. After each galvanostatic discharge for a fixed number of hours, the open circuit potential was measured with a computer-controlled potentio-galvanostat (Technologue, Inc., μ-PS/GS). At the moment the electrode potential reached steady state (in our estimation, a potential change of $<1.0 \times 10^{-6}$ V/min), equilibrium between the H atmosphere and H activity inside the Pd was believed to be attained. This operation was continued from several tens to 100 times. In each figure the abscissa indicates the H concentration, which is given by the summation of each increment of the concentration $(C_2 - C_1)$, given in accordance with Faraday's law by

$$C_1 - C_2 = -(\Phi it/\mathrm{F})(N_\mathrm{A}/N_M) \ , \qquad (1)$$

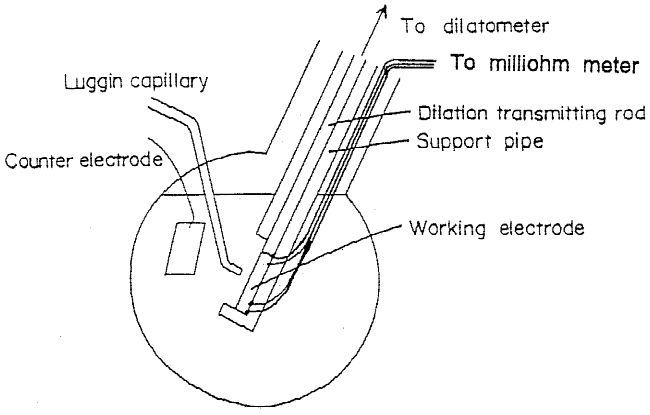

Fig. 1. Schematic of the electrolytic cell for in situ measurement of electrode potential, dilation, and resistance.

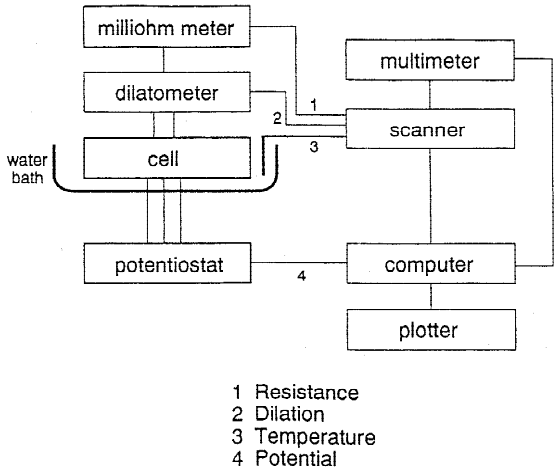

Fig. 2. Electronic apparatus for in situ measurement of potential, dilation, and resistance.

where

Φ = current efficiency

i = current

t = time of electrolysis

N_A = Avogadro's number

N_M = number of atoms of the electrode metal.

Electrolysis was performed using three types of galvanostatic trained pulse currents, as shown in Fig. 3. In applied pulse mode A, a set of pulsed currents (absorption) was applied immediately after completing the preceding set (absorption). Thus, repeated H absorption and possible desorption (during the off pulse) was continued until saturation of the H concentration was attained. The saturation of H is easily detected by the time-independent resistance if the resistance of the Pd electrode is adopted as an appropriate monitor of the H concentration.

Applied pulse mode A electrolysis was continued until H absorption saturation was reached, while in applied pulse modes B and C electrolysis, continuous cyclic absorption and desorption were performed. In applied pulse mode B, desorption was conducted by supplying a set of inverse anodic currents with an equivalent coulomb of absorption. In applied pulse mode C, desorption was conducted by applying potentiostatic conditions at the H dissolution potential (up to ~0.9 V) until complete recovery of the initial resistance of the specimen. The difference between applied pulse modes B and C is in the form of the current supply, i.e., galvanostatic pulsed current and potentiostatically controlled current. During each electrolysis the decision to supply the next absorption current was based on the diagnosis of complete recovery of the initial resistance. The experimental details have been described in Refs. 9 and 10.

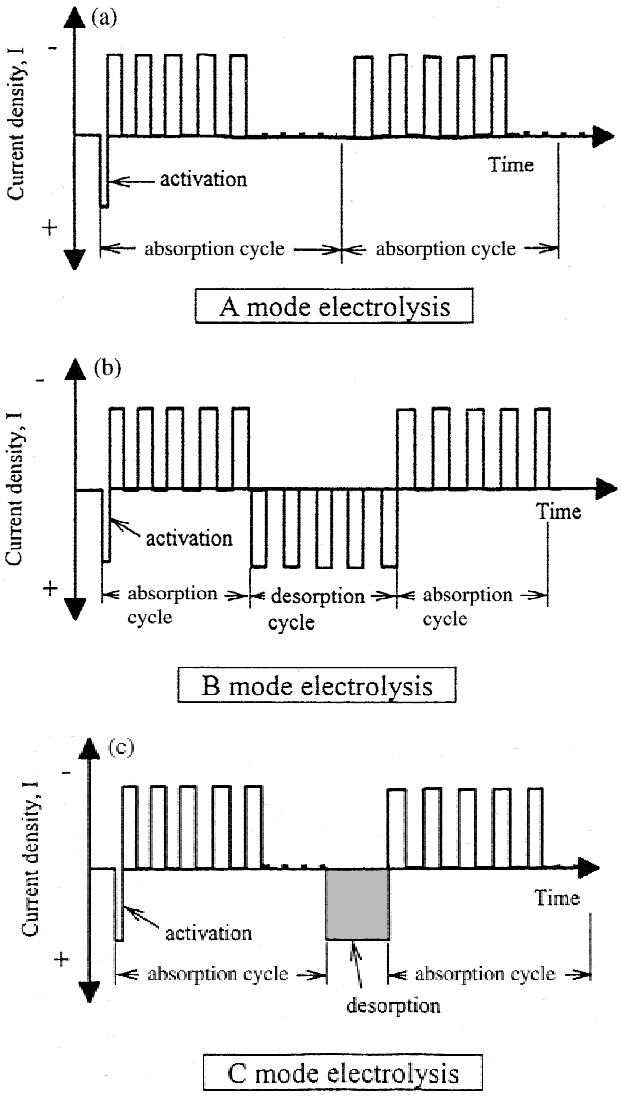

Fig. 3. A, B, and C applied pulse mode patterns of current density-time.

III. RESULTS AND DISCUSSION

III.A. Microstructure of a Plate and a Thick Pd Electrode During Deuterium Evolution in 0.1 *M* LiOD

III.A.1. Deuterium Absorption in a Pd Plate Electrode

Electrolytic absorption of H in a metal proceeds through adsorption, infusion, and diffusion, where the absorbate, H atoms on a metal surface, are generated by cathodic reduction of H ions in an aqueous solution. Although an electrode inherently has microstructural defects, such as dislocations, and twin and stacking faults, their creation and propagation have often been observed during H migration. During microscopic observation of H absorption in Pd, it is important to study H

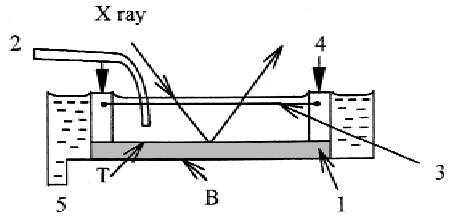

Fig. 4. Schematic of the electrolytic cell for deuterium charging on one side of a Pd plate electrode in 0.1 *M* LiOD.

migration behavior in connection with the electrode geometry (shape and volume) and under miscellaneous electrolysis conditions.

In a preliminary experiment, Numata et al.[12,13] reported that extreme bending of a Pd plate (0.3 mm thick, 30 × 40 mm), having only one side in contact with the electrolyte (T side) and the other surface free (B side), occurred during repeated deuterium absorption runs. Figure 4 shows the electrolytic cell for deuterium charging on one side of a Pd plate electrode in 0.1 *M* LiOD. Figures 5a and 5b show the X-ray diffraction (XRD) patterns of sides T and B for charges of 170 and 350 C/cm^2. For the first charge of 170 C/cm^2, an evolution of the β phase on the T side is observed resulting in $\alpha + \beta$ coexistence, while the B side shows the single α phase. During subsequent charging the inversion of the peak intensity of the α phase to the β phase occurs on the T side, and the β phase appears on the B side as schematically shown in Fig. 6. For more than 520 C/cm^2 both the T and B sides show the single β phase. Thus, the single α phase, the $\alpha + \beta$ phase coexistence, and the final single β phase occurred successively from the T to the B side as time elapsed. Figure 6 illustrates four sequential stages of the phase distribution in a Pd plate electrode during deuterium charging on one side. At the moment of bending, due to extension stress on the T side, a compression stress was induced on the B side, thus preventing deuterium migration. Consequently, further deuterium migration on the T side resulted in breakdown of the B side wall (see stage IV in Fig. 6). Scanning electron microscopy (SEM) showed traces of deuterium eruption,[12,13] which indicates an intense increase in the internal pressure (see Fig. 7). Thus, the electrolysis (one side deuterium shuttle combined with confinement on the other side, i.e., generating bifacial stress shown with opposite signs) successfully trapped deuterium in a metal as schematically shown by the modified Gorsky effect. In other words, in this electrolytic condition, the T side is in contact with a solution creating extension stress, and the B side is free creating compression stress, which provides a barrier to deuterium migration. The formation of a barrier layer during deuterium evolution also appears in the following thick-rod Pd electrode case.

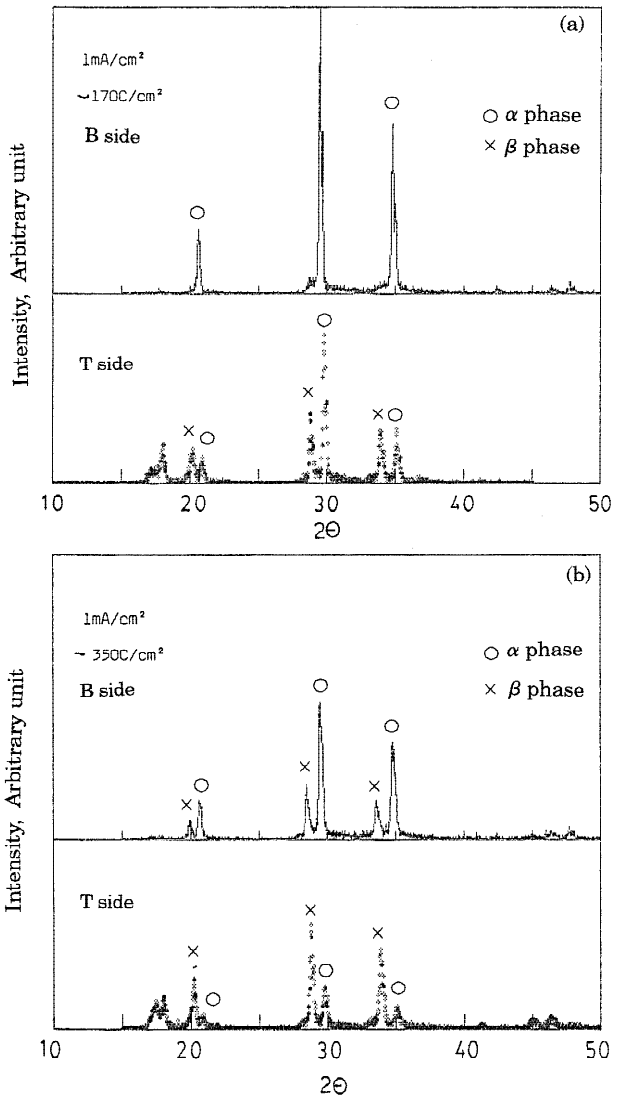

Fig. 5. The XRD patterns of sides T and B: (a) 170 C/cm^2, (b) 350 C/cm^2.

III.A.2. Microstructure of a Thick Pd Rod Under Long-Term Electrolysis in 0.1 M LiOD

Microscopic observation of a postelectrolysis Pd surface (20-mm diameter, 32 mm long) after long-term electrolysis in 0.1 *M* LiOD shows no crack but marked blisters and two long faults.[8] Figure 8 shows the morphologies of the long fault and holes around a fault. The microstructure of the Pd electrode consists of two large grains in the interior and columnar grains with random orientations near the surface, as shown in Fig. 9 (the blanket/hatched area).

The formation of the microscopic holes and faults on the Pd surface is connected to the grain structure grown

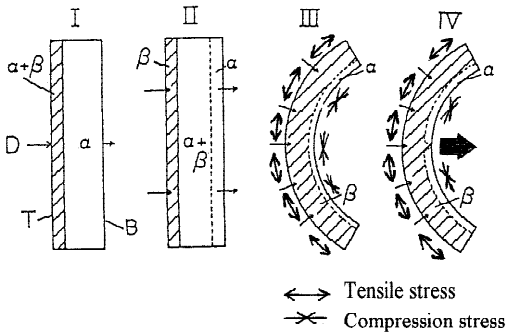

Fig. 6. Schematic of the evolution of bending when a single surface of the electrode is in contact with the electrolyte.

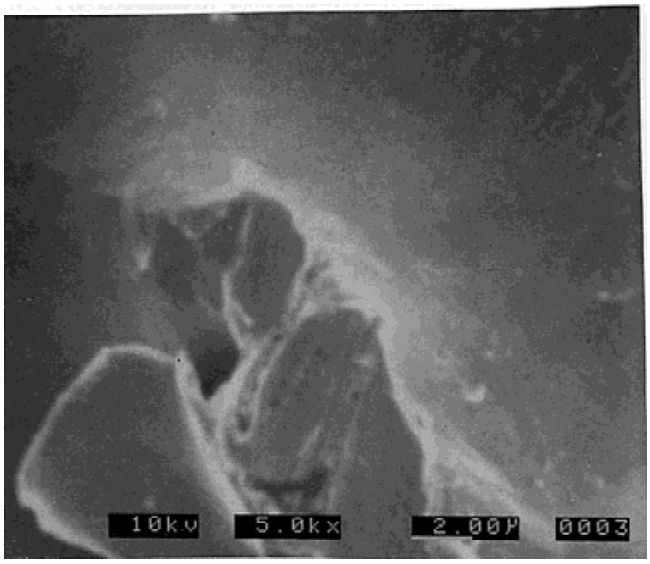

Fig. 7. SEM of a Pd plate electrode surface showing a hole on side B.

in the Pd electrode. During the first charge, the blanket (columnar grains near the surface) of the Pd rod behaves like the T side, through which deuterium absorption proceeds. An increase in current density induces compression stress in the blanket, similar to Fig. 6, which acts like a wall to compress the interior. Since the blanket might act as a barrier layer for deuterium dissipation, compression of the blanket effectively raises the pressure of the interior.

Figure 9 shows that, disregarding the geometric scale, the morphological characteristics of postelectrolysis Pd (Fig. 9b) are similar to earth's geothermal phenomena, such as volcanic eruptions and faults (Fig. 9a). Geologic analysis shows that a volcanic eruption and an earthquake depend on movement of the mantle and a huge release of heat from the earth's interior.[8] Recently, the Kobe earthquake was categorized as the active-fault type, which appeared as a trace of faults on the ground. Charged-particle emissions were reported before the earthquake and were confirmed by the analysis of a jet-like cloud, which evolved vertically from the ground. Hence, it is quite reasonable to conceive that the charged-particle emission observed was a precursor to giant ground slippage that generated faults on the surface. Let us consider the microscopic faults observed on the Pd electrode. The anomalous emission of charged particles, i.e., a kind of geothermal phenomenon, has been identified with similar emission products frequently recognized as evidence of the cold fusion phenomenon. It is presumed that the charged particles and the fusion reaction debris were the result of accidental fault formation due to the induced strain on the electrode's surface during deuterium absorption (see Fig. 9).

A model approach makes possible a valid guideline for understanding a complicated phenomenon. Numata[14–16] developed a microscopic model inside the

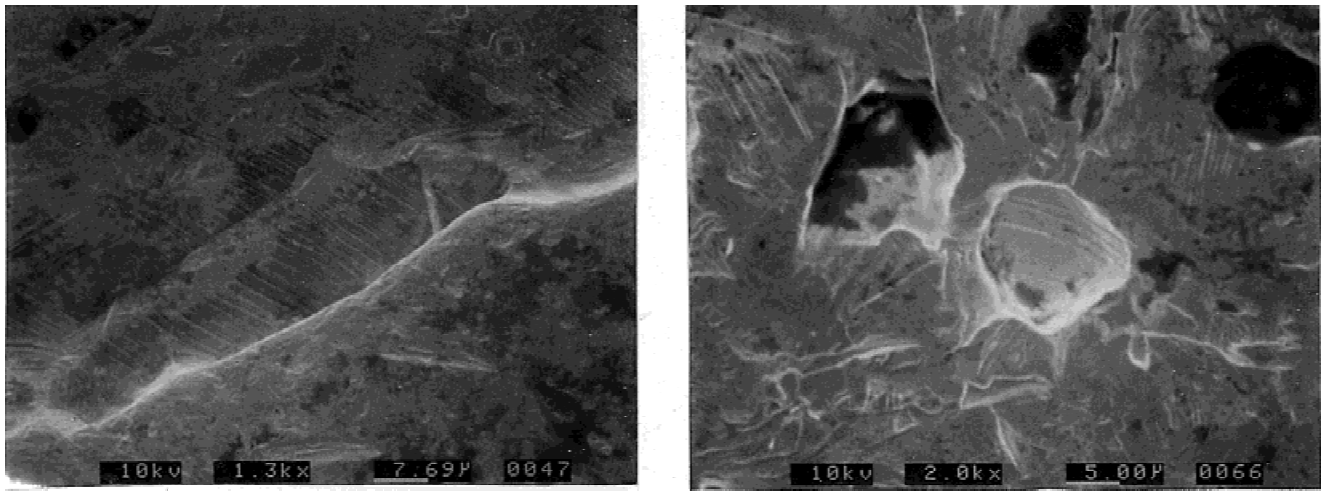

Fig. 8. SEM of a postelectrolysis Pd surface showing the exposed terrace along the fault and holes.

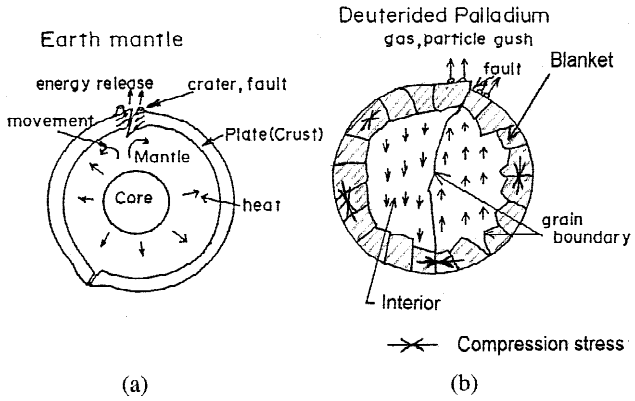

Fig. 9. Mechanism of surface holes formed along the fault of a Pd rod during long-term electrolysis in 0.1 *M* LiOD.

solid (see Fig. 10), which helped improve the reproducibility of cold fusion–related phenomena, i.e., heat evolution and emission of nuclear reaction products. Although a precise description of the model is not provided in this paper, the important concept is the cycling of four sequential processes (some of them yet remain speculative in this paper), on which in situ measurement of the physical and mechanical properties of Pd might throw some light.[16]

Among many metal-hydrogen alloys, Pd is particularly known as an easily absorbing and dissolving metal, which implies that the formation of a surface layer (e.g., Ti-H, Zr-H, and Nb-H systems) does not play a significant role as a permeability barrier.[17] However, repetition of absorption and desorption alters the microstructure more or less; therefore, loading behavior is influenced not only by surface conditions but also by bulk. Recently, significant differences in the $\alpha \rightarrow \beta$ phase change between the Pd film and the bulk suggest that the volume of a specimen plays a significant role in the physical and mechanical properties,[16] e.g., the resistance and dilation of Pd. Hence, it is interesting to explain the physical and mechanical properties of Pd in connection with microstructural changes. For this we use a rather thick Pd rod as an electrode to achieve more sensitive measurements of the bulk properties, although much longer electrolysis is required to reach a steady state of diffused H in the Pd rod.

III.B. In Situ Potentiometric, Resistance, and Dilatometric Measurements of Pd Under Single Absorption

III.B.1. Hydrogen Evolution and Absorption in Pd

The H evolution reaction (HER) on Pd in an acidic solution takes place through the Volmer reaction followed by the Heylovsky one [Eqs. (2) and (3)] or the Volmer reaction followed by the Tafel one [Eqs. (2), (3), and (4)]:

$$\text{Volmer reaction: } H^+ + e^- = H_{ad} \tag{2}$$

$$\text{Heylovsky reaction: } H_{ad} + H_{ad} + e^- = H_2 \tag{3}$$

$$\text{Tafel reaction: } H_{ad} + H_{ad} = H_2 \tag{4}$$

$$\text{Infusion: } H_{ad} \rightarrow H_{ab} \ , \tag{5}$$

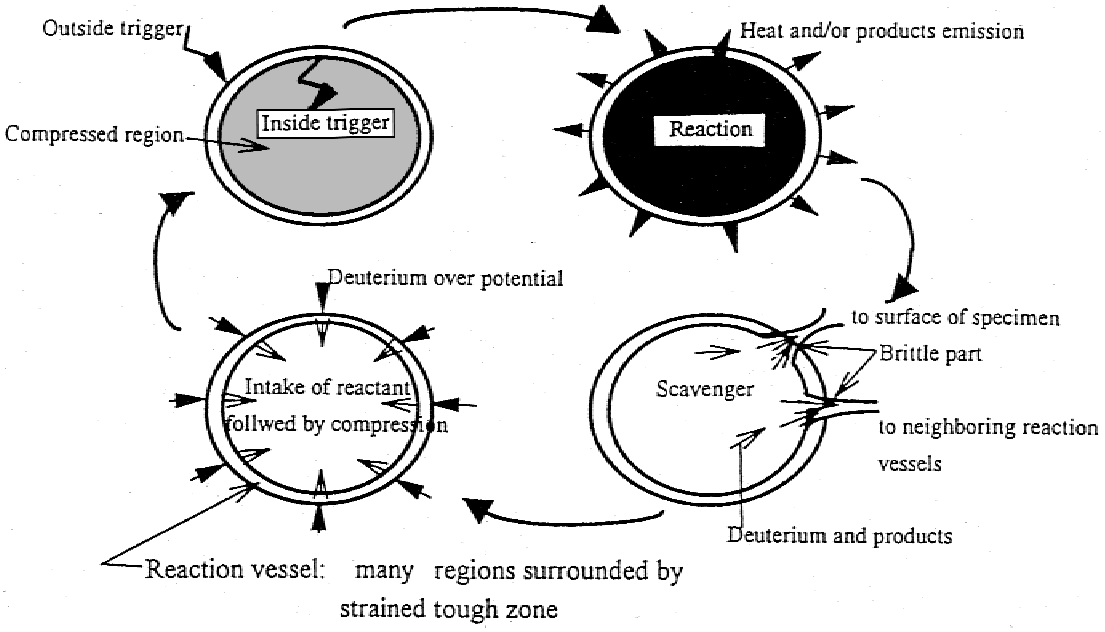

Fig. 10. Schematic of a nuclear reaction cycle model.

where H_{ad} and H_{ab} denote H adsorbed on and absorbed in an electrode. From the Tafel slopes obtained by the current-interruption method,[9] the rate-determining step of the HER is the Eq. (4) Tafel step in these experimental conditions.[9]

Parallel to the consumption of the adsorbed H through the recombination reaction [Eq. (3) or Eq. (4)], the adsorbed H fills interstitial sites forming the single α phase. The maximum concentration attainable was evaluated in several papers,[18] taking into account the absorption and desorption of H; however, more detail on this point is beyond the scope of this paper. The H concentration in this paper can be conveniently expressed as x:H/Pd (atomic ratio), where the absorption efficiency of adsorbed H is given as 100% for $x < 0.55$ (at 40°C) and almost 80% for $x > 0.6$. On the other hand, when the current density is low enough, infusion of the adsorbed H atoms, which is given by Eq. (5), is faster than that of the Tafel reaction [Eq. (4)], and H loading is performed with a current efficiency of 100%. Here, the HER on Pd at current densities <10 mA/cm^2 is treated as completely dissolved, which is in good agreement with other reports.[19–21] Note that since an elongation and an electrode potential were measured simultaneously, electrolysis was conducted with lower current densities (<10 mA/cm^2) to suppress the thermal expansion caused by the electrolysis.

III.B.2. In situ Potentiometric, Resistance, and Dilatometric Measurements of a Pd Electrode Under Single Absorption

Figure 11 shows a plot of the in situ measurements of potential, resistance, and dilation changes as a function of H/Pd ratio, where the Pd electrode (2-mm diameter, 50 mm long) was first loaded by the A applied pulse mode electrolysis. The change in resistance and dilation is given by the ratio of the measured values to the initial ones (indicated by the subscript 0). In Fig. 11, α_{max} is the limit of the α phase, β_{min} is the limit of $\alpha + \beta$ phase coexistence, β_{tr} is the transition from the β phase to $\beta + PdH_{2-x}$, V_{min} is the onset of the β + void coexistence region, and R_{tr} is the transition from increasing resistance to a damped one and defined as the value of the H/Pd ratio corresponding to the H dissipation triggered. The lower inserts show α single, $\alpha + \beta$ coexistence, β single, and β + void coexistence phase regions, where the corresponding microstructures are schematically illustrated.

Figure 12 shows a replot of the potential change as a function of logarithmic H concentration at 40°C during the first absorption experiment. When the H on the electrode surface and that within the electrode are in equilibrium,

$$E = E^\circ - \mathrm{RT/F} \ln a_{\mathrm{H}ab} - 2.3\mathrm{RT/F}\cdot\mathrm{pH} \ . \qquad (6)$$

Accordingly, the Nernst equation can be written as

$$E = E^\circ - \mathrm{RT/F} \ln a_{\mathrm{H}ab} - 0.248 \ , \qquad (7)$$

where $a_{\mathrm{H}ab}$ represents the activity of H atoms. The other symbols have their usual meanings. For $x \leq 0.01$ the electrode potential obeys Nernst Eq. (7) showing a straight line with a slope of -2.3 RT/F. The results evidently reveal that the electrode potential is in accordance with the Nernst equation in this range of concentration, and the potential is controlled by the reaction given in Eq. (2).

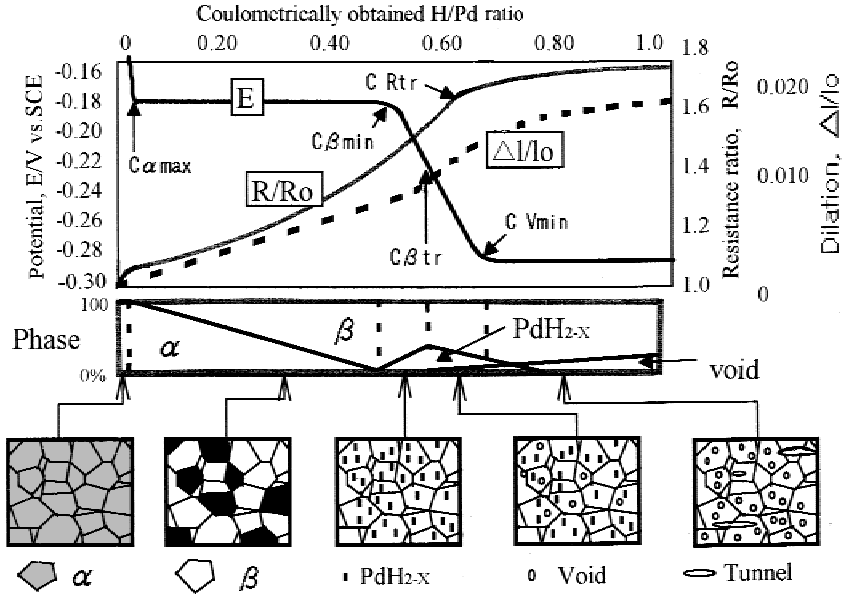

Fig. 11. Schematic of the evolution of various phases and voids, the A applied pulse mode potential, dilation, and resistance ratio, as a function of H/Pd ratio during cathodic absorption of H in Pd.

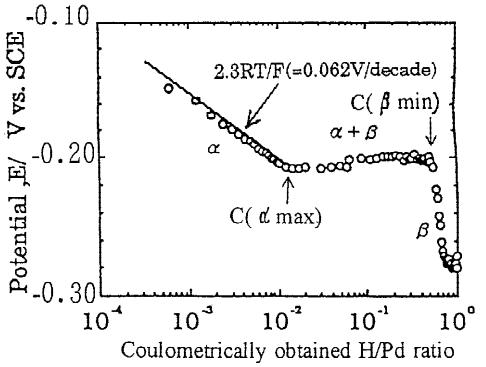

Fig. 12. Applied pulse mode A potential as a function of the logarithm of H/Pd ratio at 40°C.

When the H/Pd ratio exceeds 0.01, the electrode potential becomes constant within the $\alpha + \beta$ phase coexistence region. The appearance of the β phase indicates two-phase coexistence; i.e., the $\alpha + \beta$ has been established. In the case of two-component, three-phase coexistence, the degree of freedom is 1 from Gibbs' phase rule. Therefore, when the concentration changes, the H potential remains constant. Since the H pressure and potential are equivalent, as described later, the pressure also remains constant. When the H/Pd ratio exceeds 0.55, the single β phase is established, and the electrode potential again begins to change in a mean direction in accordance with Gibbs' phase rule.

The change of potential in the single β phase is not allowed to obey Nernst's Eq. (7) with a slope of -2.3 RT/F. It has been expected that interaction among H atoms becomes strong. However, on inspecting the potential as a function of H/Pd ratio curve (see Fig. 12), it is apparent that it shifts progressively to a less-noble direction until it reaches the limiting value (i.e., totally distinct from the Nernstian behavior), which is similar to the transition from one state to a new one. Alternatively, kinetic analysis[22] of deuterium absorption in Pd showed that the electrode surface is covered by a new phase (designated the gamma phase) with a high deuterium concentration. In view of the following results, in situ measurements suffice to give a comprehensive understanding of the behavior of the potential change:

1. The potential begins to shift toward a less-noble direction, and the increasing resistance concurrently begins to level out, indicating that the absorbed H is not responsible for an increase in the resistance (i.e., their existence in the lattice sites), and the H is thus distributed in voids as molecular H.

2. A steep rise of the dilation occurs in this range of concentration, where the potential begins to decrease, i.e., the equivalent H pressure increases. Precise calculations of the apparent molar volume showed a sudden up-and-down movement within a narrow range of concentration, where an unstable PdH_2 precipitate (acting finally as the nuclei of voids) is involved in a shrunken β phase. Hence, a consistent explanation for the potential shift above 0.55 is that it is due to void formation with a volume of $(\frac{1}{3})\Delta l/l_0$. The formation of voids was further confirmed by SEM observation (see Figs. 22a and 22c).

Let us think of the H gas in a gas phase that is in equilibrium with the H within an electrode. Using the activity of the H within the electrode, the pressure of the H can be calculated from the electrode potential under limited conditions[9,23]:

$$pH_2^{eq} = \exp[-(E + E_{SCE})(2F/RT)] \ , \qquad (8)$$

where E_{SCE} is the potential of the reference electrode. Thus, the equivalent H pressure, pH_2^{eq}, the H pressure equilibrated with that in the Pd matrix (e.g., in a void), is expressed assuming the Nernst equation. The equivalent H pressure at more than $x = 0.01$ in accordance with Eq. (8) is plotted in Fig. 13. The $\alpha + \beta$ phase coexistence pressure, 0.05×10^5 Pa, coincides with that obtained from the Pd-H isotherm at 40°C. When the state is turned into the single β phase, the equivalent H pressure again begins to increase until a final pressure of 16×10^5 Pa has been reached.

When the H/Pd ratio x is increased to >0.8, the potential becomes constant, and the H is thought not to be dissolved any further. Occlusion of H in the Pd electrode by electrolysis can be said to be limited to ~ 0.8. Rosamilia et al.[24] obtained the H dissolution limit by a rotating disk electrode method and have reported that $PdH_{0.81}$ is the largest component. When the maximum concentration is achieved, it is believed that adsorbed H atoms react faster by the Tafel process than by the process in which the atoms are dissolved within the electrode.

These characteristic values [the values of α_{max} and β_{min} of the phase transition and $pH_2^{eq}(\alpha + \beta)$] are consistent with those of the Pd-H isotherm obtained by the

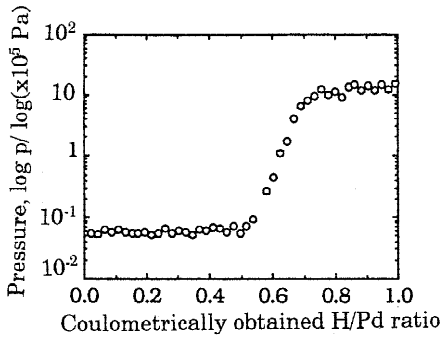

Fig. 13. Equivalent H pressure as a function of the H/Pd ratio at 40°C; $\alpha + \beta$ coexistence phase pressure is 0.05×10^5 Pa.

gas equilibrium method, which adds weight to the observation that the average values give results consistent with a system having a uniform composition between the surface and the interior.

III.B.3. Elastic Interaction Between Pd and Absorbed H

It is known that interaction between dissolved atoms and surrounding materials often bring about lattice strain in materials. This lattice strain is a cause of the miscibility gap of phase transformation or the leaning plateau region in the Pd-H isotherm. Think of the case of n H atoms being dissolved in N metal atoms.[25] If we assume that the volume of one metal atom and that of one H atom are Ω_M and Ω_H, respectively, then the volume of the metal and the hydrogen are given as

$$V_M = N \cdot \Omega_M \ , \quad V_H = n \cdot \Omega_H \ . \tag{9}$$

For 1 g of atom,

$$V_M = N_A \cdot V_M, \ V_H = N_A \cdot V_H \ , \tag{10}$$

where V_M and V_H are the molar volumes of the metal and the hydrogen, respectively. The volumetric ratio of expansion is given by

$$\Delta V / V_M = (n \cdot \Omega_H)/(N \cdot V_M) \ , \tag{11}$$

where Ω_H is the volume change due to H infusion.

When the H is dissolved at random in a cubic system, the following equation is obtained, provided that the volume change is small:

$$\Delta V / V_M = 3 \cdot (\Delta l / l_0) + 0 \cdot [3 \cdot (\Delta l / l_0)] + \cdots \ . \tag{12}$$

By combining the preceding with Eq. (11),

$$\Delta l / l_0 = (x \cdot \Omega_H)/3 \cdot \Omega_M) = (x \cdot V_H)(3 \cdot V_M) \ ; \tag{13}$$

i.e.,

$$V_H = 3 \cdot V_M \cdot [d(\Delta l / l_0)/dx] \ . \tag{14}$$

By measuring the slope of the H/Pd ratio of dilation, the molar volume of H in a material can be obtained. The dilation as a function of H/Pd ratio in the α phase is plotted in Fig. 14a and was measured simultaneously with the case shown in Fig. 12. The dilation is almost in proportion to an increase in the H/Pd ratio, and using Eq. (14), the molar volume of H is obtained as V_H = 1.64 cm^3/mol with the supposition that V_{Pd} = 8.87 cm^3/mol. The result agrees with values from the literature, V_H = 1.77 to 1.06 cm^3/mol (Ref. 26). From this we can derive that the H atoms amount to 3.7×10^{24} occluded atoms per cubic centimetre, and this is two orders of magnitude larger than the value for liquid H 4.2×10^{22}.

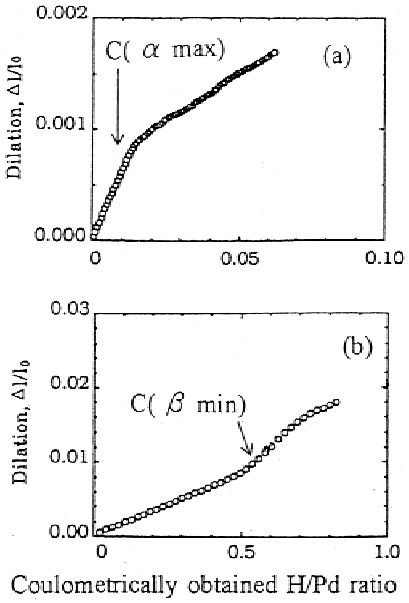

Fig. 14. Dilation ($\Delta l/l_0$) as a function of H/Pd ratio: (a): $x <$ 0.06, 40°C, 0.5 mA, 2000 s; (b) $x <$ 0.8, 40°C, 5 mA, 7000 s.

III.B.4. The Relationships Between Potential, Dilation, and Resistance Changes Under the A Applied Pulse-Mode Electrolysis

As shown in Fig. 11, the potential decreases with increasing H/Pd ratio within the single α phase and reaches a constant value corresponding to the $\alpha + \beta$ phase coexistence. Meanwhile, the resistance monotonically increases showing a slight deviation from exact proportionality to the H/Pd ratio. Although the resistance curve is ambiguous at very low concentrations, resistance rises steeply, and the slope of the resistance as a function of H/Pd ratio changes to a small value at the onset of the $\alpha + \beta$ phase. For $x > 0.55$ the slope in the resistance curve begins to decrease and levels off at the point of inflection (R_{tr}). Furthermore, it approaches a limiting value of 1.8 for $x > 0.80$. This behavior appeared only in the first absorption of the A applied pulse mode. The samples subjected to repeated H absorption and desorption exhibited almost the same behavior up to the β phase, but above R_{tr} they flatten at 1.7 (see Fig. 20b). The difference in the resistance behavior above R_{tr} is attributed to the contribution of unrecovered absorbed H. Thus during the first absorption and desorption, a small volume of H remained trapped near the surface even after annealing at 1100°C. The volume at the surface, whose interstitial sites are already occupied, do not, therefore, contribute to the resistance change.[27] It is reasonable to assume that the H in the remaining sites is readily dissolved and absorbed by the electrochemical reaction, and the slow resistance

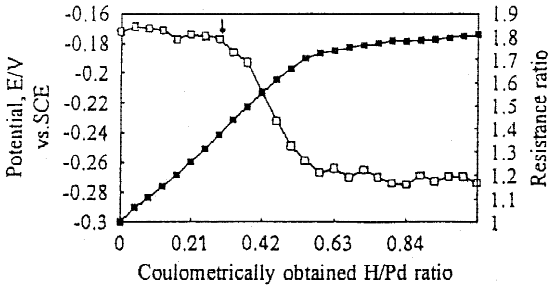

Fig. 15. The A applied pulse-mode potential and resistance ratio as a function of H/Pd ratio, 40°C after 30 h holding (at arrow) Pd was again electrolyzed. Potential (—□—), resistance ratio (—■—).

increase above R_{tr} was not observed during subsequent absorption runs. The maximum limiting values of 1.7 and 1.8 obtained are consistent with those of bulk Pd ranging from 1.65 to 1.8 (Refs. 28, 29, and 30).

Under electrolysis at <10 mA/cm^2, the transient of the dilation was almost proportional to the charging time, and the initial length was recovered by conducting an anodic oxidation reaction. On the other hand, no less than half the dilation was recovered in the case of desorption at 5 mA/cm^2. Hence, the dilation behavior can be sensitive to the inherent structural properties as well as to the electrolysis conditions. For example, the dilation as a function of the H/Pd ratio in the α phase revealed an equilibrium between fault-free crystal and H, while the β phase evolution considerably deformed the β phase.

Plots of dilation as a function of the H/Pd ratio are shown in Fig. 14a ($x < 0.06$) and Fig. 14b ($x < 0.8$). The β phase has a larger lattice constant than the α phase (4%), although the slope is smaller in the $\alpha + \beta$ phase coexistence than in the α phase. Assuming that the slopes with respect to the H/Pd ratios correspond to the average values of the α phase and β phase lattice constants, both of which are inversely weighed by the individual volume ratios, the values of $a(\alpha_{max}) = 3.893$ and $a(\beta_{min}) = 3.929$ Å can be obtained assuming the Pd lattice constant $a(0)$ is 3.890. The values coincide with the reported ones, $a(\alpha_{max}) = 3.894$ and $a(\beta_{min}) = 4.025$ Å (Ref. 31).

Thus, $a(\beta_{min}) = 3.929$ estimated from the tangential value at β_{min} was considerably smaller than the value obtained from gas equilibrium experiments. This suggests that the electrolytically formed β phase in the α phase matrix possesses heavily strained regions with a small average lattice constant. Such deformed regions might stimulate void nucleation under high pressure, resulting in potentially less-noble shifts. The void formation reaction is further described later. When the β single phase was attained, large dilation linearly proportional to the H/Pd ratio up to $x = 0.8$ was seen. These results agree with the reports[25,32] that the dilation or the volume expansion appear to be linearly proportional to the H/Pd ratio up to $x = 0.8$.

In Fig. 11 the potential shifted to a new phase of PdH_2 and voids formed in the β matrix. At the transition, the dilation ($\Delta l/l_0$) increased abruptly and decayed progressively to a small value. The abrupt increase in dilation accompanying the potential transition is thought to be due to unstable PdH_2 precipitation and its transition to voids in the crystal.

III.C. Repeated Absorption and Desorption of H in Pd

III.C.1. Repeated Absorption and Desorption of H in Pd Under Applied Pulse Mode A

Two repetitions of the A applied pulse mode (2-mm diameter, 50 mm long) were performed, and the time dependence of the resistance was examined by interrupting the electrolysis. Figure 15 shows the first potential and resistance plot as a function of the H/Pd ratio, where the intervention is indicated by the arrow. The time dependence of the resistance was for 30 h within the experimental uncertainty. As the figure shows, the potential and resistance behavior were essentially the same as the first A applied pulse-mode electrolysis irrespective of interruptions. Since the H/Pd ratio at the interventions exhibits an equivalent H pressure of the $\alpha + \beta$ coexistence region (0.05×10^5 Pa), evidently no H was released under a pressure of 1atm.

On the other hand, Fig. 16 shows typical potential and resistance changes as a function of the H/Pd ratio for the repeated A applied pulse-mode electrolysis without any electrochemical desorption but subjected to a spontaneous desorption for several minutes. Although the two limiting potentials of the two phase coexistence regions ($\alpha + \beta$) and (β + void) were -0.18 and -0.28 V, respectively, and were within the acceptable deviation, the values of β_{min} and the onset of the β + void

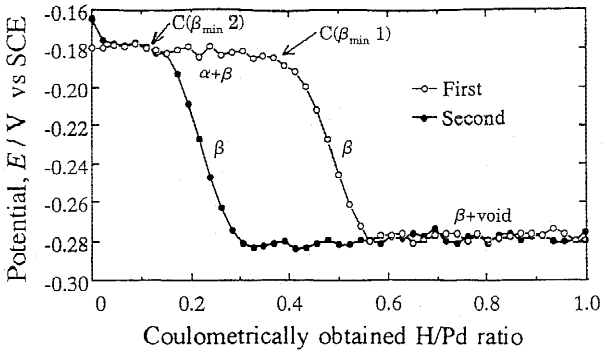

Fig. 16. The A applied pulse-mode potential as a function of H/Pd ratio of first and second repetitions at 40°C and current density of 0.5 mA/cm^2. The specimen was again electrolyzed under the same conditions as the first absorption.

coexistence region (V_{min}) appreciably decreased with an increase in the number of repetitions. Thus, the second absorption proceeds, on the contrary, by offsetting the remaining H concentration on the H/Pd ratio axis, which is consistent with an equivalent H pressure of 1.6×10^6 Pa, which is more than atmospheric pressure. The exact value of the remaining concentration was estimated by superimposing the second curve on the first one offset by $x = 0.26$. Thus, a spontaneous desorption occurs in which the β + void coexistence region is attained, exhibiting an equivalent H pressure of 1.6×10^6 Pa. These results, including the examination during the interruption in the α phase, are reasonable evidence that the equivalent H pressure is due to hydraulic pressure inside the electrode.

It is inferred that the spontaneous desorption during the A applied pulse-mode electrolysis exhibits no influence on the H absorption condition, in contrast to the well-accepted concept that the electrochemical absorption/desorption proceeds accompanied by an evolution of miscellaneous lattice defects on a matrix.

III.C.2. Repeated Absorption and Desorption of H in Pd ($x < 0.02$) in the B Applied Pulse Mode

Repeated absorption and desorption of H (0.8-mm diameter, 50 mm long, 0.2 mA/cm^2, 7000 s) was performed in the B applied pulse mode ($x < 0.02$), where the H/Pd ratio was controlled up to the onset of the α-β transition: α_{max}. In this case H infusion was not expected to have any influence on the mechanical properties because the diffusion of H proceeds rapidly and without an appreciable $\alpha \rightarrow \beta$ phase transformation. There is no significant deterioration in the mechanical properties from desorption repetition because the diffusion of H proceeds rapidly and without hysteresis to the α phase matrix. The results of the first through fourth repetitions of absorption and desorption show that the electrode potential obeys the Nernst equation while the potential shifts toward a less-noble direction as the number of repetitions is increased. The plots of the potential as a function of H/Pd ratio of the fifth through the eleventh repetitions show steep straight lines; thus, the onset of the phase transition proceeds at a much smaller H/Pd ratio than that of the first run. The equivalent H pressure of the $\alpha + \beta$ phase is increased, accompanied by an evolution of potential fluctuations. The features of a large number of repetitions reveal that even a low level of absorption influences the potential shift to less-noble values. This involves the mechanical effect, e.g., stress or H association, as evidenced by the increased and unstable pressure variations.

The dilation as a function of H/Pd ratio curves is shown in Fig. 17, where the slopes of the second through fourth repetitions increase progressively; most of the slopes after the fifth repetition tend to converge into one line. For all the repetitions except the first, an induction

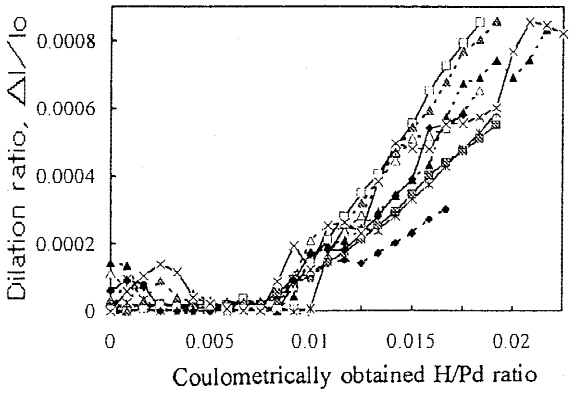

Fig. 17. Effect of number of repetitions on B applied pulse-mode dilation as a function of H/Pd ratio ($x < 0.02$). Dilation: 2nd (—◆—), 3rd (—*—), 4th (- -△- -), 5th (—▧—), 6th (- -▲- -), 7th (- -*- -), 8th (—□—), 9th (- -◬- -), 10th (- -◆- -), 11th (—×—).

period of the dilation appeared where the α single phase exists. Inspecting the dilation as a function of the H/Pd ratio curves and taking into account the uncertainty in the experiment, it is reasonable to assume that the dilation ($\Delta l/l_0$) is composed of the linear term of the lattice expansion and the complemental term as follows:

$$\Delta l/l_0 = ax + b \quad a\text{:constant} \ , \tag{15}$$

where the first term on the right side corresponds to the change of dilation due to lattice expansion, and the second term is attributable to sporadic dilation (discontinuous to H/Pd ratio and time). The latter is also observed under work hardening on a single crystal. Although it is questionable that a Pd rod under repeated absorption and desorption behaves like a heavily strained crystal, we often observe such sporadic and stepwise dilation under electrochemical loading. It is highly possible to evaluate the progress of the critical condition in terms of the amplitude and/or frequency of the second term.[16]

The results of the resistance ratio (R/R_0) as a function of H/Pd ratio show a monotonic increase with increasing H/Pd ratio, where the effect of the number of repetitions lies within a maximum experimental uncertainty. The resistance behavior suggests that H is readily mobile in spite of the fact that the dilation varied with the number of repetitions and the appearance of the induction period.

Table I summarizes the results of repeated absorption and desorption in the B ($x < 0.02$) and C ($x < 0.8$) applied pulse modes. For example, the resistance behavior for the B applied pulse-mode electrolysis shows no distinct dependence on the number of repetitions, while the resistance ratio as a function of H/Pd ratio in the C applied pulse mode exhibits a totally different dependence on repetition number. In the C applied pulse mode, the resistance ratio shows a steady increase and flattens

TABLE I

Results of Repeated Absorption and Desorption in the B and C Applied Pulse Modes

Electrolysis Condition		Potential, $E - \log(\mathrm{H/Pd})$	Resistance Ratio, $(R/R_0) - \mathrm{H/Pd}$	Dilation, $(\Delta l/l_0) - \mathrm{H/Pd}$
Mode	H/Pd Ratio			
B	<0.02 (c.d. 0.2 mA/cm^2)	1st through 4th Nernstian 5th through 11th deviation from Nernstian	No hysteresis	2nd through 4th increased slope, 5th through 11th no cycle effect
C	<0.8 (c.d. 0.2 and 2 mA/cm^2)	Data scattered but much deviated from Nernstian	Large hysteresis	Data not available

out at $R/R_0 = 1.7$ as the H/Pd ratio increases. During a few of the repetitions, the H/Pd ratio at the edge of the plateau shifts toward a higher content.

III.D. The A Applied Pulse-Mode Electrolysis with Intervening Anodic Desorption and Void Formation

Figure 18a shows plots of the potential and dilation changes, and Fig. 18b shows plots of the resistance and apparent partial molar volume $[d(\Delta l/l_0)/dx]$ changes as a function of H/Pd ratio under the first A applied pulse-mode electrolysis. Here, the apparent partial molar volume (abbreviated as apparent molar volume) was calculated from $3V_M$ multiplied by the slope of the dilation as a function of H/Pd ratio plots [Eq. (14)]. The value of a single phase gives the molar volume of the corresponding phase, and for a two-phase coexistence, the apparent molar volume is weighted by the individual volumetric ratios. The molar volumes of hydrogen are 1.64 cm^3/mol (α phase Pd) (Ref. 9), PdH_n ($1 \le n \le 3$) (Ref. 33); PdH 10.8, PdH_2 7.25, PdH_3 5.15 cm^3/mol, 1.77 to 1.06 cm^3/mol (Ref. 26). Note that the molar volume of voids contained in the matrix is disregarded because no volume expansion occurs through the absorption, although this is not the case for the molar volume of voids at the first absorption.

The values of the apparent molar volume obtained from Fig. 18b are 1.64 cm^3/mol for the single α phase and 0.4 cm^3/mol for the $\alpha + \beta$ phase coexistence. For two-phase coexistence the values do not vary with increasing H/Pd ratio, where the absorption presumably occurs in a homogeneous structure free from voids and cracks and the like, in contrast to the C applied pulse mode. The potential in Fig. 18a shows Nernstian behavior (α phase), the constant value of the $\alpha + \beta$ phase coexistence, the transition toward a less-noble direction ($\beta_{min} \sim V_{min}$), and the next constant value of the β + void coexistence where the apparent molar volume follows two constant values corresponding to the α and $\alpha + \beta$ phases coexistence (1.64 and 0.4 cm^3/mol), then a sharp rise to $\sim$1.2 at β_{min} followed by a drop and subsequent slow decrease. The peak of the apparent molar volume corresponds to the abrupt increase (at β_{min}) and to the progressive damping in dilation. This peak is at the transition from the apparent molar volume recovery region to the new state (designated as β_{tr}). In Figs. 18a and 18b the onset of the potential shift β_{min} and that of β + void coexistence region V_{min} coincide with the onset and the end of the peak response of the dilation. Therefore, the less-noble potential shift ranging from -0.8 to -1.0 V

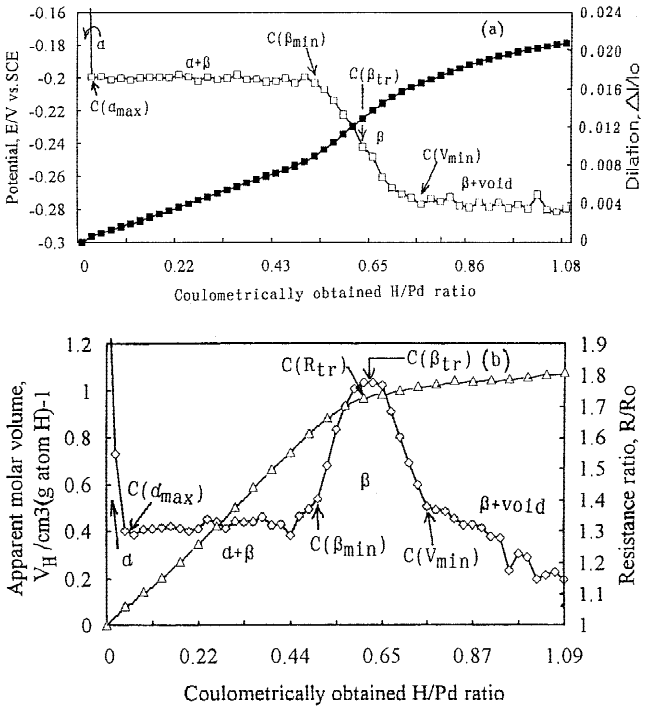

Fig. 18. The A applied pulse-mode potential, dilation, resistance, and apparent molar volume as a function of H/Pd ratio of the first absorption at 40°C. (a) Potential (—□—) and dilation (—■—) as a function of H/Pd ratio; (b) resistance (—△—) and apparent molar volume (—◇—) as a function of H/Pd ratio.

is intimately related to anomalous H absorption, resulting in the sharp rise of the apparent molar volume. In other words, by increasing the equivalent H pressure, $0.05 \rightarrow 16 \times 10^5$ Pa, the apparent molar volume increases to 1.2 and recovers to 0.4, and concurrently above R_{tr}, the resistance increases asymptotically toward 1.8 (β_{tr}).

If the H absorption assumes the well-known Pd-H isotherm, the potential shift obeys Nernst's equation, and the resistance continues to increase steadily, showing a recovery of the apparent molar volume to 1.64 cm^3/mol. However, the experimental data did not show ideal behavior; hence, the following new interpretation has been drawn. Since the value of the peak (1.2 cm^3/mol) was lower than 1.64 cm^3/mol (absorption in octahedral sites of Pd) and apart from ideal absorption the potential shifts to less-noble values, the predominant absorption of the octahedral sites above β_{min} is disturbed by a fine precipitate of PdH_{2-x} ($0 < x \leq 1$) due to the occupation of tetrahedral sites. Then, through β_{tr} the increased pressure allows the unstable precipitates to decompose to PdH_{1-x} and H gas [Eq. (16)]. For such a nonequilibrium process, in situ measured data can provide a valid explanation:

$$PdH_{2-x} \rightarrow PdH_{1-x} + 1/2H_2$$

$$PdH_{2-x}\text{: tetrahedral sites occupation} \quad . \qquad (16)$$

On this occasion H evolution in the matrix causes void formation.

Above R_{tr} (between β_{tr} and V_{min}) the apparent molar volume drops concurrently with the transition from PdH_{2-x} precipitation to absorption in voids when the resistance curve levels off (see Fig. 18b). Here, resistance did not respond to void formation. The existence of voids that are larger than that of the mean free path of conduction electrons is not sensitive to the resistance because the resistance increase is due to the scattering of conduction electrons subjected to H absorption. The lower insets in Fig. 11 illustrate the unstable PdH_{2-x} precipitation followed by void formation associated with the irregular potential shift toward a less-noble direction and the peak of the apparent molar volume. Such a new phase different from the β phase is proposed by Mizuno et al.[22] and Storms.[18]

With the appearance of PdH_{1-x} and voids, there were two equilibrium phases, including PdH_{2-x}, and the potential shift ceased at 16×10^5 Pa, obeying the phase rule. Meanwhile, the resistance invariance between β_{tr} and V_{min} exhibited no further absorption, and it is reasonable to say that the absorption above V_{min} followed the application of an insignificant amount of overpotential. These results are consistent with the view of the onset of H migration paths through whole surfaces to cracked surfaces. Storms[18]reported that the amount of H dissolved balances with that absorbed with deformed β phase formation described later. Again, the resistance did not respond to the formation of external cracks, considering the cracks opened diametrally.

As a result, the dilation due to isotropic dissolution is composed of elastic and plastic deformation, internal voids, and cracks, as shown in Eq. (17):

$$\begin{aligned} \Delta l/l_0 (>\beta_{min}) = {} & \text{elastic and plastic elongation} \\ & + \tfrac{1}{3}\ \text{(voids volume)} \\ & + \tfrac{1}{3}k\ \text{(crack volume)} \end{aligned} \qquad (17)$$

with k, 0 to 1; axial cracks, 0; diametral cracks, 1.

III.E. Repeated Absorption and Desorption of H in Pd ($x < 0.8$) in the C Applied Pulse Mode

The same absorption and desorption of H was repeated in the C applied pulse mode (0.8-mm diameter, 50 mm long, 7000 s) where the electric charge of absorption was more than that required to attain a H/Pd ratio of 1.0.

Figures 19a and 19b show the absorption behavior of the second and third repetitions in the C applied pulse mode. Comparing the values of the limiting $\alpha + \beta$ phase coexistence ($\beta_{min}2$, $\beta_{min}3$) to those of the first A applied pulse mode shows that these increase, in contrast to the first A applied pulse mode, with an increasing number of repetitions. Furthermore, in the later stages of the $\alpha + \beta$ phase coexistence, the dilation seems to be intermittent, showing abrupt drops in the apparent molar volume (see Fig. 19b), whereas the potential, dilation, and resistance behave similarly to those described previously. Figure 19b shows the resistance and apparent molar volume of the third repetition of the C applied pulse mode together with that of the A applied pulse mode (open square symbols). In the enlarged $\alpha + \beta$ phase coexistence region, the apparent molar volume decreased considerably, and the resistance increased with an increase in the H/Pd ratio. The point at which the absorption-dilation correlation is temporarily broken off is termed the "breathing mode." Such a peculiar phenomenon also appeared within the α phase in the B applied pulse mode during the induction period of the dilation under the usual progressive absorption. During this induction period, the H absorption causes a nonuniform dilation with the formation of a strain volume. In the C applied pulse mode, in the $\alpha + \beta$ phase coexistence region, the H absorption proceeds inhomogenously, showing an apparent molar volume of 0.6 to 0.8 cm^3/mol and a subsequent lower apparent molar volume of 0.32 to 0.08 cm^3/mol. The latter lower molar volume suggests that H was absorbed in the high-density defect areas surrounding voids, which were introduced by the preceding absorption/desorption repetitions. The areas of high-defect density are characterized by the lower apparent molar volume, 0.32 to

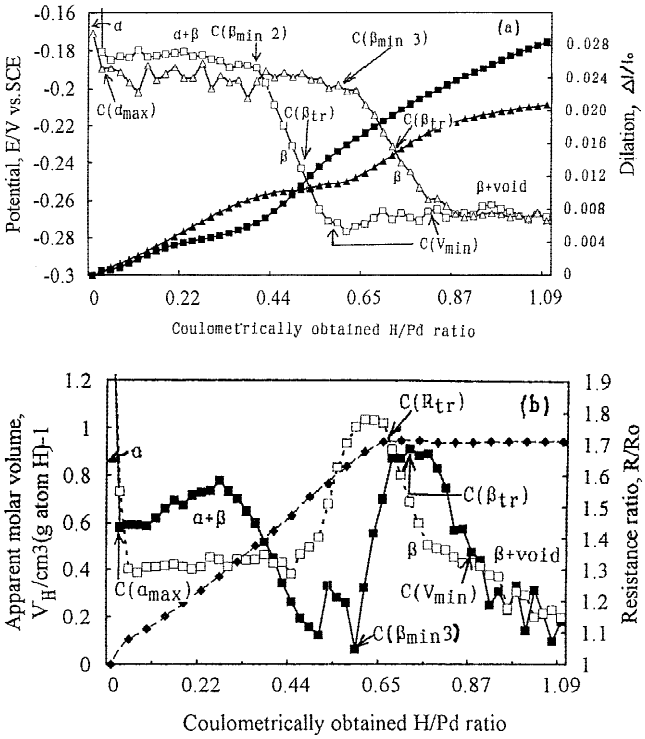

Fig. 19. The C applied pulse mode potential, dilation, resistance, and apparent molar volume as a function of H/Pd ratio of the second and third absorption at 40°C. (a) Potential, second (—□—), and third (—△—) absorptions, dilation of second (—■—) and third (—▲—) absorptions; (b) resistance (—◆—) and apparent molar volume of third (—■—) and first (—□—) absorptions.

0.08 cm^3/mol, whose volumetric ratio tends to increase with an increase in the number of repetitions. As a result, above β_{min} the volumetric ratio of voids (third repetition) was 1.6%, assuming the corresponding dilation is purely due to void formation.

During the A, B, and C applied pulse modes, in situ measurement of these variables was necessary for a comprehensive understanding of the microstructural changes due to H absorption/desorption.

III.F. Effect of Number of Repetitions on Void Formation in the C Applied Pulse Mode with Intervening Anodic Oxidation Reaction

The values of β_{min} and R_{tr} increased with repeated absorption and desorption where the incremental charge in the H/Pd ratio corresponds to the charges for these voids reaching the equivalent H pressure. The dependence on repetition of the potential and resistance as a function of H/Pd ratio is shown in Figs. 20a and 20b. The resistance curves level off 1.7 at R_{tr}, and the potentials exhibit two constant values corresponding to the $\alpha + \beta$ phase and β + void coexistence regions. Figure 21 shows the dependence of the values of β_{min} and R_{tr} on the number of repetitions. These values tend to approach saturation, which does not yet appear in the figure. Since the first absorption does not require the corresponding charge, the incremental value from each repetition is equal to that of the absorption in the voids and high-density areas. Then the volumetric ratio required for voids is evaluated to be ~9, assuming the equivalent H pressure is 0.05×10^5 Pa, while those obtained from the dilation as a function of H/Pd ratio curves range from 1.6 to 2.4%. Hence, the incremental amount of the H/Pd ratio is attributable to the charge by absorption in high-defect density areas having lower apparent molar volume.

Figures 22a, 22b, and 22c show scanning electron micrographs of the surface and cross-sectional areas of the Pd electrode subjected to C applied pulse-mode electrolysis. A crack grown along the axis and voids opened at the inner surface of a crack are shown in Fig. 22a. The morphology observed in Fig. 22b shows that voids and surface grooves have a short migration path, contributing to the fast attainment of equilibrium.

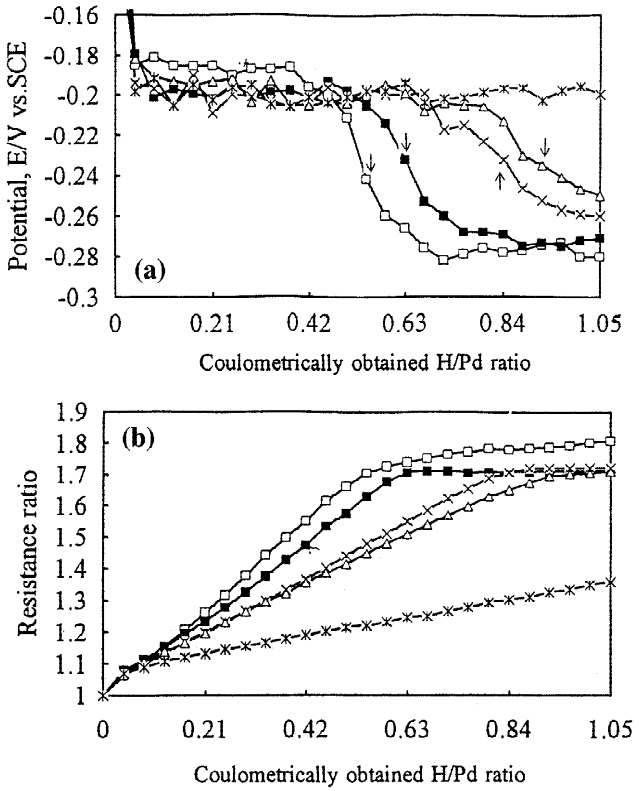

Fig. 20. Effect of the number of repetitions on the C applied pulse mode potential and resistance as a function of Pd/H ratio at 40°C. (a) Potential, first (—□—), second (—■—), third (—X—), fourth (—△—), fifth (—*—); (b) resistance, first (—□—), second (—■—), third (—×—), fourth (—△—), fifth (—*—).

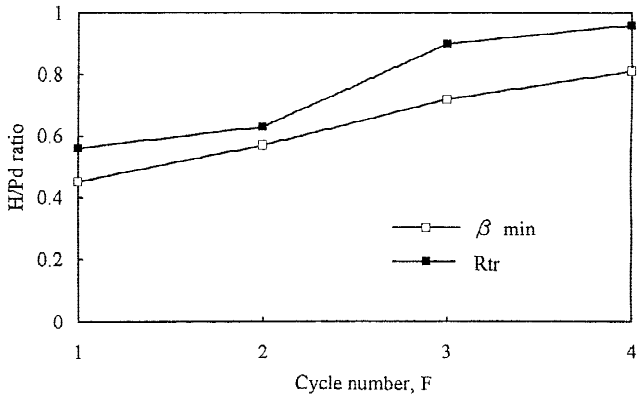

Fig. 21. Effect of number of repetitions on characteristic values of β_{min} and R_{tr} at 40°C.

Figure 22c shows the locus of voids (arrows), which are visualized by cutting the specimen. These microscopic observations support void formation during the C applied pulse mode as suggested by the resistance and dilation data analysis.

III.G. Two Types of H Electrode Characterized Above V_{min}

Two types of Pd electrode used in electrolytic H absorption are described in Table II. The H confined electrode (blanket structure) holds high-pressure H in a cell whose wall is formed by a step-by-step increasing current supply in 0.1 *M* LiOD. The resulting characteristics were a potential as high as −2.44 V and voids, faults, and slip bands appearing on the surface during long-term absorption. Finally, the electrode encountered catastrophic high pressure under long-term HER. The electrode might behave like a cell surrounded by a tough wall, which might enable the establishment of cold fusion conditions.

The H dissipation electrode is formed by conduction, i.e., the C applied pulse mode in an acidic solution, where the surface voids and cracks are readily observable and are accompanied by the H evolution reaction through cracks (designated as the H pumping action). The important parameters determining the local stress of a specimen are the electrolysis mode, the solution, the electrode geometry, and the pretreatments as listed in Table II. Therefore, the effect of local stress on H behavior once it has been absorbed is taken into account.

Storms[18] first confirmed that the amount of H absorbed over the whole surface balanced with that dissolved through the cracks. This view is consistent with the view that the dilation continues to increase, whereas resistance ceased to increase. Thus, R_{tr} is defined as the value of the H/Pd ratio corresponding to the H triggered (H pumping action). In Fig. 20a the arrows show the potential correlated with R_{tr} in the range from 0.641 to 1.0×10^5 Pa. Hence, when the equivalent H pressure

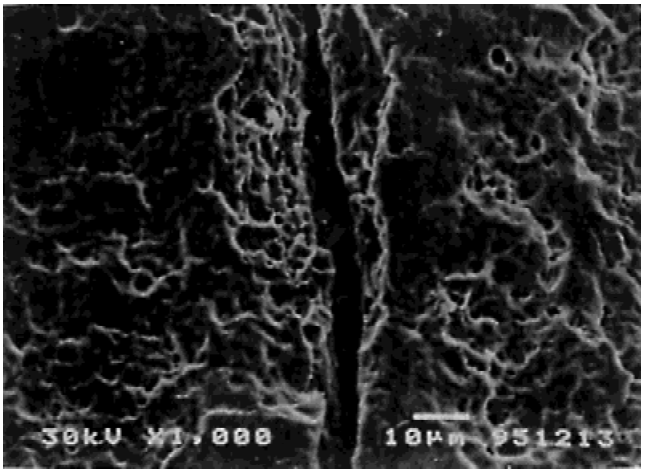

(a)

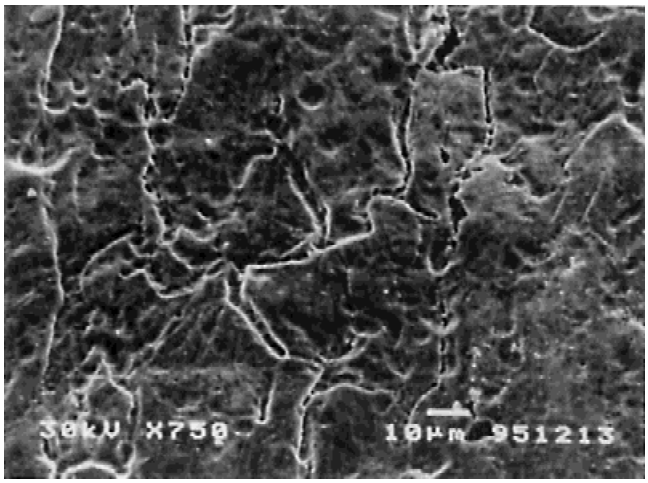

(b)

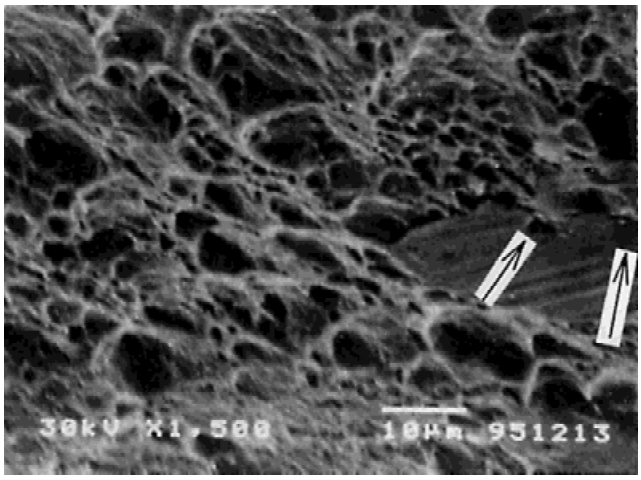

(c)

Fig. 22. (a) and (b) Scanning electron micrographs of Pd electrode surface. (c) Cross-sectional area in which the area cut by a knife appears to be flat.

TABLE II

Characteristics and Electrolysis Conditions of a Typical Hydrogen Electrode

Type	Hydrogen Dissipation Electrode	Hydrogen Confined Electrode
Pretreatment	Annealing	Casting, annealing, preloading in D_2
Electrolysis	C applied pulse mode	Increase of current step by step
Solution	Glycerine + H_3PO_4	0.1 *M* LiOD
Geometry	Thin plate, thin rod	Thick rod
Finally reached potential (V)	−0.28 V (versus SCE)	−2.44 [versus $(\alpha + \beta)$−PdD]
Morphology	Void, crack	Surface void, slip band, two long fault blanket structure, tunnel
Local stress	(Tensile)	Compression
H behavior	Dissipate from cracks (H pumping action)	Confined (blanket structure)

exceeds atmospheric pressure, above R_{tr}, the absorbed H easily dissipates, resulting in the limit of the H/Pd ratio.

IV. CONCLUSION

We summarize our study as follows:

1. A thick Pd rod under long-term electrolysis in 0.1 *M* LiOD contained two large grains and coarse columnar grains, where the latter provide a barrier layer for deuterium dissipation and a wall. The formation of the characteristic microstructure was explained as similar to miscellaneous geologic phenomena, such as earthquake and active fault formation.

2. For $x \leq 0.01$, in the single α phase the electrode potential obeyed the Nernst equation, and it exhibited a constant value within the $\alpha + \beta$ coexistence region. For $x > 0.55$ in the single β phase the potential shifted to a less-noble direction accompanied with a steep rise of the dilation. In the single β phase an unstable PdH_{2-x} precipitate decomposed to PdH_{1-x} and voids in the β matrix. The characteristic values of α_{max}, β_{min}, $pH_2^{eq}(\alpha + \beta)$, with V_H were consistent with those of the Pd-H isotherm obtained by the gas equilibrium method.

3. During the A applied pulse mode after saturation, further enhancement of the H/Pd ratio was impossible by duplication. In contrast, the sample absorbed in the β phase was subject to spontaneous dissipation.

4. During the B applied pulse mode ($x < 0.02$), the electrode potentials of the first through fourth repetitions shifted to a less-noble direction, while those of the fifth through eleventh repetitions showed steep straight lines, i.e., non-Nernstian behavior. The slopes of the dilation as a function of H/Pd ratio increased progressively, and most of the slopes after the fifth repetition converged into one line.

5. During the C applied pulse mode, the $\alpha + \beta$ phase coexistence region was enlarged, and the incremental H/Pd ratio corresponded to H absorption in high-density defect areas surrounding voids. SEM observation showed voids inside the Pd rod electrode.

6. Comprehensive understanding of the changes of the potential, the resistance, and the apparent molar volume provides insight into the microstructure of the thick Pd rod electrode during H absorption/desorption repetition.

7. The H (deuterium) confined electrode formed by conducting long-term electrolysis in 0.1 *M* LiOD was compared with the H dissipation electrode formed by conducting, for example, C applied pulse-mode electrolysis in an acidic solution.

ACKNOWLEDGMENTS

This work was partially supported by the New Hydrogen Energy Project, New Energy Development Organization, and the Institute of Applied Energy, Japan. The authors would like to thank T. Ooi of Ube Company for experimental help. They would also like to express sincere thanks to the late R. Takagi of the Tokyo Institute of Technology and M. Fukuhara of Toshiba Tungaloy Company, Kawasaki, Japan, for their insightful discussions.

REFERENCES

1. M. FLEISCHMANN and S. PONS, "Electrochemically Induced Nuclear Fusion of Deuterium," *J. Electroanal. Chem.*, **261**, 301 (1989).

2. S. E. JONES et al., "Observation of Cold Nuclear Fusion in Condensed Matter," *Nature*, **338**, 737 (1989).

3. A. DE NINNO, A. FRATTOLILLO, G. LOLLOBATTISTA, and F. SCARAMUZZI, "Evidence of Emission of Neutrons from a Titanium-Deuterium System," *Europhys. Lett.*, **9**, 221 (1989).

4. H. O. MENLOVE, M. M. FOWLER, E. GARCIA, M. C. MILLER, M. A. PACIOTTI, R. R. RYAN, and S. E. JONES, "Measurements of Neutron Emission from Ti and Pd in Pressurized D_2 Gas and D_2O Electrolysis Cells," *J. Fusion Energy*, **9**, 495 (1990).

5. T. MIZUNO, T. AKIMOTO, and N. SATO, "Neutron Evolution from Annealed Palladium Cathode in LiOD-D_2O Solution," *Denki Kagaku*, **57**, 742 (1989).

6. H. NUMATA and M. FUKUHARA, "Low-Temperature Elastic Anomalies and Heat Generation of Deuterated Palladium," *Fusion Technol.*, **31**, 300 (1997).

7. R. TAKAGI, H. NUMATA, I. OHNO, K. KAWAMURA, and S. HARUYAMA, "Neutron Emission During a Long-Term Electrolysis of Heavy Water," *Fusion Technol.*, **19**, 2135 (1991).

8. H. NUMATA, R. TAKAGI, I. OHNO, K. KAWAMURA, and S. HARUYAMA, "Neutron Emission and Surface Observation During a Long-Term Evolution of Deuterium on Pd in 0.1MLiOD," *Proc. Conf. Science of Cold Fusion*, Vol. 33, ACCF2, Como, Italy, June 29, 1991, p. 71, T. BRESSANI, E. DEL GIUDICE, and G. PREPARATA, Eds., SIF, Bologna, Italy (1991).

9. T. OOI, H. NUMATA, and I. OHNO, "Electrochemical Solution of Hydrogen in Palladium and Dilation of Electrode," *Denki Kagaku*, **61**, 324 (1993).

10. H. NUMATA, T. OOI, and I. OHNO, "In-Situ Potentio Dilatometric Measurement of Hydrogen Absorption in Pd Electrode by Electrochemical Cathodic Loading Method," *Extended Abstracts Electrochemical Society, Spring Mtg.*, Honolulu, Hawaii, July 4, 1993, Vol. 93-1, p. 2419, Electrochemical Society (1993).

11. R. KIRCHHEIM, "Interaction of Hydrogen with Dislocations in Pd-1. Activity and Diffusivity and Their Phenomenological Interpretation," *Acta Metall.*, **29**, 835 (1981).

12. H. NUMATA, R. TAKAGI, I. OHNO, K. KAWAMURA, and S. HARUYAMA, "Neutron Emission During Deuterium Evolution on Pd in Heavy Water," *Proc. Fall Mtg. Electrochemical Society of Japan*, p. 157, The Electrochemical Society of Japan (1989).

13. H. NUMATA, R. TAKAGI, I. OHNO, K. KAWAMURA, and S. HARUYAMA, "Neutron Emission During Deuterium Evolution on Pd in Heavy Water," *Proc. Mini Symp. Cold Fusion*, Tokyo Metropolitan University, p. 129 (1990).

14. H. NUMATA and I. OHNO, "Hydrogen Behavior in Pd During Repeated Electrochemical Hydrogen Absorption and Desorption," *Proc. 3rd Symp. Basic Research Group in New Hydrogen Energy Project*, Tokyo, Japan, July 3, 1996, p. 55, The Institute of Applied Energy (1996).

15. H. NUMATA and I. OHNO, "Evaluation of Effect of Material Characteristics on Absorption of Deuterium in Pd," *1995 Report of Basic Research Group in New Hydrogen Energy Project*, IAE-C9513 p. 302 (1996).

16. H. NUMATA and I. OHNO, "In Situ Potentio, Resisto and Dilatometric Measurement of Repeated Hydrogen Absorption in Pd Electrode by Electrochemical Cathodic Loading Method," *Proc. 6th Int. Conf. Cold Fusion, Progress in New Hydrogen Energy*, Toya, Japan, October 13, 1996, Vol 1, p. 213, NEDO, The Institute of Applied Energy (1997).

17. T. MIZUNO and M. ENYO, "Sorption of Hydrogen on and in Hydrogen-Absorbing Metals in Electrochemical Environments," *Modern Aspects of Electrochemistry*, No. 30, p. 480, R. E. WHITE et al., Eds., Plenum Press, New York (1996).

18. E. STORMS, "Formation of β-PdD Containing High Deuterium Concentration Using Electrolysis of Heavy-Water," *J. Alloys Compounds*, **268**, 89 (1998).

19. T. B. FLANAGAN and F. A. LEWIS, "Hydrogen Absorption by Palladium-Hydrogen System," *Trans. Faraday Soc.*, **55**, 1400 (1959).

20. T. B. FLANAGAN and F. A. LEWIS, "Electrode Potentials of the Palladium-Hydrogen System," *Trans. Faraday Soc.*, **55**, 1409 (1959).

21. R. T. FALLON and G. W. CASTELLAN, "The Mechanism of Occlusion of Hydrogen by Palladium Contact with Sulfuric Acid Solution," *J. Phys. Chem.*, **64**, 4 (1960).

22. T. MIZUNO, T. AKIMOTO, K. AZUMI, and M. ENYO, "Diffusion Rate of Deuterium in Pd During Cathodic Charging," *Denki Kagaku*, **60**, 405 (1992).

23. H. ZÜCHNER and H. G. SCHÖNEICH, "Improvement of Electrochemical Methods for Studying the Diffusion and Solubility of Hydrogen in Metals," *J. Less-Common Met.*, **101**, 363 (1984).

24. J. R. ROSAMILIA, J. A. ABYS, and B. MILLER, "Electrochemical Hydrogen Insertion into Palladium and Palladium-Nickel Thin Films," *Electrochim. Acta*, **36**, 1203 (1991).

25. H. PEISL, "Lattice Strains Due to Hydrogen in Metals," *Hydrogen in Metals*, Vol. 1, p. 53, G. ALEFELD and J. VÖLKL, Eds., Springer, Berlin (1978).

26. R. FEENSTRA, R. GRIESSEN, and D. G. DE GROOT, "Hydrogen Induced Lattice Expansion and Effective H-H Interaction in Single Phase PdH_c," *J. Phys. F: Met. Phys.*, **16**, 1933 (1986).

27. K. KANDASAMY, F. A. LEWIS, and S. G. McKEE, "Hydrogen Chemical Potentials and Phase Transitions in Palladium Black Electrodeposits," *Surface Coating Technol.*, **35**, 93 (1988).

28. B. BARANOWSKI, S. MAJCHRZAK, and T. B. FLANAGAN, "The Volume Increase of fcc Metals and Alloys Due to Interstitial Hydrogen over a Wide Range of Hydrogen Contents," *J. Phys. F: Metal. Phys.*, **1**, 258 (1971).

29. F. A. LEWIS, W. D. McFALL, and T. C. WITHERSPOON, "Hysteresis of Pressure-Composition and Electrical Resistance-Composition Relationships of Pd/H and Pd Alloy/H Systems," *Z. Physik. Chem. Neue Folge*, **114**, 239 (1979).

30. M. NICOLAS, L. DUMOULIN, and J. P. BURGER, "Thickness Dependence of the Critical Solution Temperature of Hydrogen in Pd Films," *J. Appl. Phys.*, **60**, 3125 (1986).

31. E. WICKE and H. BRODOWSKY, "Hydrogen in Palladium and Palladium Alloys," *Hydrogen in Metals*, Vol. 2, p. 73, J. VÖLKL and G. ALEFELD, Eds., Springer, Berlin (1979).

32. J. E. SCHIRBER and B. MOROSIN, "Lattice Constants of β-PdH_x and β-PdD_x with x near 1.0," *Phys. Rev. B*, **12**, *1*, 117 (1975).

33. A. C. SWITENDICK, "Electronic Structure and Stability of Palladium Hydrogen (Deuterium) Systems, $PdH(D)_n$, $1 \leq n \leq 3$," *J. Less-Common Met.*, **172–174**, 1363 (1991).

Hiroo Numata (Dr Eng, materials engineering, Tokyo Institute of Technology, 1979) is a research associate at Tokyo Institute of Technology. His current research activities are involved with the kinetic study of molten carbonate fuel cell electrode reactions, incineration of wastes in molten salt, and analysis of metal hydrogen systems.

Izumi Ohno (Dr Eng, applied electrochemistry, Tokyo Institute of Technology, 1971) is a former professor at Tokyo Institute of Technology. Her research interest is electrochemistry of electro- and electroless deposition of metals and alloys.